UC Davis
UC Davis Previously Published Works

Title

Electric field—guided collective motility initiation of large epidermal cell groups

Permalink

Journal

ISSN

Authors

Sun, Yaohui
Reid, Brian
Zhang, Yan
et al.

Publication Date

DOI

Peer reviewed

Electric field–guided collective motility initiation of large epidermal cell groups

Yaohui Sun[a,b,*], Brian Reid[a], Yan Zhang[a,†], Kan Zhu[a], Fernando Ferreira[a,c], Alejandro Estrada[a], Yuxin Sun[a,‡], Bruce W. Draper[d], Haicen Yue[e], Calina Copos[f], Francis Lin[g], Yelena Y. Bernadskaya[b], Min Zhao[a,*], and Alex Mogilner[b,*]

[a]Department of Ophthalmology and Vision Science and Department of Dermatology, School of Medicine, University of California, Davis, Sacramento, CA 95817; [b]Courant Institute and Department of Biology, New York University, New York, NY 10012; [c]Departamento de Biologia, Centro de Biologia Molecular e Ambiental (CBMA), Universidade do Minho, 4710-057 Braga, Portugal; [d]Department of Molecular and Cellular Biology, University of California, Davis, Davis, CA 95616; [e]Department of Physics, Emory University, Atlanta, GA 30322; [f]Department of Biology and Department of Mathematics, Northeastern University, Boston, MA 02115; [g]Department of Physics and Astronomy, University of Manitoba, Winnipeg, MB R3T 2N2, Canada

ABSTRACT Recent research has elucidated mechanochemical pathways of single cell polarization, but much less is known about collective motility initiation in adhesive cell groups. We used galvanotactic assays of zebrafish keratocyte cell groups, pharmacological perturbations, electric field switches, particle imaging velocimetry, and cell tracking to show that large cell groups initiate motility in minutes toward the cathode. Interestingly, while PI3K-inhibited single cells are biased toward the anode, inhibiting PI3K does not affect the cathode-directed cell group migration. We observed that control groups had the fastest cathode-migrating cell at the front, while the front cells in PI3K-inhibited groups were the slowest. Both control and PI3K-inhibited groups rapidly repolarized when the electric field direction was reversed, and the group migration continued after the electric field was switched off. Inhibiting myosin disrupted the cohesiveness of keratocyte groups and abolished the collective directionality and ability to switch direction when the electric field is reversed. Our data are consistent with a model according to which cells in the group sense the electric field individually and mechanical integration of the cells results in coherent group motility.

INTRODUCTION

Cells migrate collectively as cohesive groups during embryonic development, wound healing, and tumor metastasis (Friedl and Gilmour, 2009; Scarpa and Mayor, 2016). Cell coordination within cohesive groups and collective directional response to external cues underlies crucial biological and pathological processes, and understanding respective mechanisms is a pressing problem. Most research on collective cell migration has been focused on groups moving in response to chemical gradients (Theveneau et al., 2010; Dona et al., 2013; Shellard et al., 2018) or on edges of in vitro wounds where cells move into free space. However, multiple studies have shown that cells can directionally respond to other directional cues, such as applied direct current electric fields (EFs), in both in vitro and in vivo settings (Lin et al., 2008; Kennard and Theriot, 2020). In this phenomenon, termed electrotaxis or galvanotaxis,

cells migrate toward the cathode or anode of the external EF (McCaig *et al.*, 2005; Cortese *et al.*, 2014). Notably, EFs have been recorded in biological tissues during development (Shi and Borgens, 1994) and wound healing (Nuccitelli, 2003; McCaig *et al.*, 2005; Zhao, 2009). For example, disruption of epithelial integrity collapses the transepithelial potential, generating steady EFs with cathode at the wound center. These in vivo EFs drive directional migration of keratinocytes/keratocytes into the wound, resulting in cellular coverage of the wound bed—an initial reepithelialization process that is critical for skin and cornea healing (Barker *et al.*, 1982; Chiang *et al.*, 1992; Zhao *et al.*, 2006). Also notably, physiological galvanotactic signals are often as potent as, or even more powerful than, chemotactic or mechanotactic signals (Chang and Minc, 2014).

Multiple intracellular signaling pathways involving phosphatidylinositol 3-kinases (PI3Ks) (Zhao *et al.*, 2006), mitogen-activated protein kinases (MAPKs), extracellular signal–regulated kinase (ERK) (Zhao *et al.*, 2002), Rho/Rock kinases (Rajnicek *et al.*, 2006), and small G-proteins (Sato *et al.*, 2009) have been implicated in the mechanisms underlying electrotactic behaviors (Zhao *et al.*, 2006; Bonazzi and Minc, 2014). However, these pathways are shared and overlap with those modulating chemotaxis. Thus, mechanisms responsible for sensing and transducing electrical signals in motile cells remain elusive (Cortese *et al.*, 2014; Nakajima *et al.*, 2015). Fish epidermal keratocytes have been an instrumental model in studying these mechanisms due to fast and steady locomotion, simple shape, and well-understood motility mechanics of this cell type (Mogilner *et al.*, 2020). It has long been known that keratocytes respond to EF, moving toward the cathode (Cooper and Schliwa, 1986; Huang *et al.*, 2009). Physically, keratocytes likely sense EF by harnessing the electrophoresis of charged mobile transmembrane proteins, which aggregate to one side of the cell (Allen *et al.*, 2013). These redistributed components can serve either as receptors, activating intracellular signaling relays, or as scaffolds for such receptors upstream of PI3K activation and polarization (Allen *et al.*, 2013).

Comparing the galvanotaxis of zebrafish epidermal keratocytes and their subcellular fragments, we have previously concluded that protrusive actin and contractile actomyosin networks self-polarize to the front and rear of the motile cell, respectively. The electric signal orients both networks toward the cathode, but the cathode orientation of the protrusive lamellipodial front is stronger, and the cells migrate to the cathode (Sun *et al.*, 2013). Inhibiting PI3K partially disorganizes the protrusive lamellipodium (i.e., "weakening" it), so that the cathode orientation of the contracting actomyosin rear "wins" redirecting the cells to anode (Sun *et al.*, 2013). These are behaviors of the polarized motile cells, and cell motility is initiated by either spontaneous or induced polarization. Spontaneously, keratocytes polarize slowly, over tens of minutes, from the rear (Yam *et al.*, 2007; Barnhart *et al.*, 2015). An EF accelerates the motility initiation by an order of magnitude, but the cells still polarize from the rear (Sun *et al.*, 2018). Interestingly, whether PI3K is inhibited or not, the cells polarize to the cathode (the PI3K-inhibited cells then turn and move to the anode) (Sun *et al.*, 2018). On the other hand, when myosin is inhibited, spontaneous polarization is completely suppressed (Yam *et al.*, 2007; Barnhart *et al.*, 2015). EF bypasses the requirement for myosin in polarization, but myosin-inhibited cells polarized in EFs have erratic motility and irregular shapes (Sun *et al.*, 2018).

Collective keratocyte migration has received much less attention than single cell migration; however, both spontaneous migration of groups of zebrafish (Rapanan *et al.*, 2014) and goldfish (Szabo *et al.*, 2006) keratocytes and EF-induced collective movements of zebrafish (Huang *et al.*, 2009) and goldfish (Cooper and Schliwa, 1986) keratocytes have been characterized. Collective migration of other

types of cells has recently received more attention, revealing that coordinated collective cell behavior could be precisely manipulated and controlled by EFs (Li *et al.*, 2012; Cohen *et al.*, 2014; Zajdel *et al.*, 2020; Shim *et al.*, 2021; Zhang *et al.*, 2022).

Many questions about cell groups migrating in EFs remain unanswered: Do the cells sense EF individually and independently, or collectively? Are there leader and follower cells? Considering that some perturbations can reverse individual cell directionality, what would such perturbations do to the collective directionality? In this study, we investigated the movements of cohesive keratocyte groups in EF. We found that unperturbed large keratocyte groups migrate to the cathode, the same as individual cells. Surprisingly, large cohesive groups of PI3K-inhibited cells also moved to the cathode, opposite the anode-directed single PI3K-inhibited keratocytes. The speed of cells in the unperturbed and PI3K-inhibited groups was maximal at the groups' fronts and centers/rears, respectively. The groups initiate motility and reverse its direction, when EF polarity is switched, in minutes, with almost simultaneous reactions in all regions of the group. These behaviors were consistent with a qualitative model according to which the cells in cohesive groups sense EF individually and integrate mechanically to enable the whole group to move coherently.

RESULTS

Scale wound–generated electric fields initiate motility of large epidermal cell groups to the cathode

We and others have reported that EFs induce collective cell migration in cultured monolayers (Li *et al.*, 2012; Cohen *et al.*, 2014). However, testing EF-directed migration in an in vivo–derived epithelial cell group has been technically challenging (Zhao *et al.*, 2003). Pioneering work by Cooper and Schliwa (1986) has demonstrated that fish keratocyte clusters perform directional migration under direct-current EFs. Yet, the clusters they used were rather small, containing only up to 40 cells plus a greater than physiological voltage of 8 V/cm to generate motility (Cooper and Schliwa, 1985, 1986). To address these issues, we generated primary epidermal cell groups from explanted scales of zebrafish, obtaining large keratocyte groups in 24–48 h (Supplemental Figure S1, A–C). Using phase contrast and fluorescently labeled images, we calculated that these groups' size is from hundreds of microns to millimeters and contain hundreds to tens of thousands of individual cells (Supplemental Figure S1, D and E). These keratocyte groups maintained integrity through cell–cell adhesions (Rapanan *et al.*, 2014).

To define the EF range guiding epidermal keratocyte group migration in vitro, we first measured the endogenous ionic currents around scale wounds in live zebrafish using a noninvasive vibrating probe (Reid *et al.*, 2007; Huang *et al.*, 2009) (Figure 1, A–C). Upon wounding, a large outward current emerged and increased until a peak of up to 3 $\mu A/cm^2$ was reached around 1 h postwounding (Figure 1D). Despite the gradual decline, this electrical signal persisted for at least 4 h, matching the approximate time required for the reestablishment of a new epidermis, as reported in a zebrafish skin wound model (Richardson *et al.*, 2013). The mean peak outward current around the wound was 3.52 $\mu A/cm^2$, while the intact scale epithelium, outside the electrical influence of the wounds, maintained tiny currents of 0–0.19 $\mu A/cm^2$ (Figure 1E). Thus, the wound is electrically negative in relation to the surrounding tissue, establishing the cathode of the endogenous EF at the wound center, as shown by simulations (Figure 1F). Given that the measured conductivity of the medium is about 13.74 m℧/cm, a mean peak outward current of 3.52 $\mu A/cm^2$ sustains an EF of about 2.56 V/cm, as calculated per Ohm's law (*Materials and Methods*).
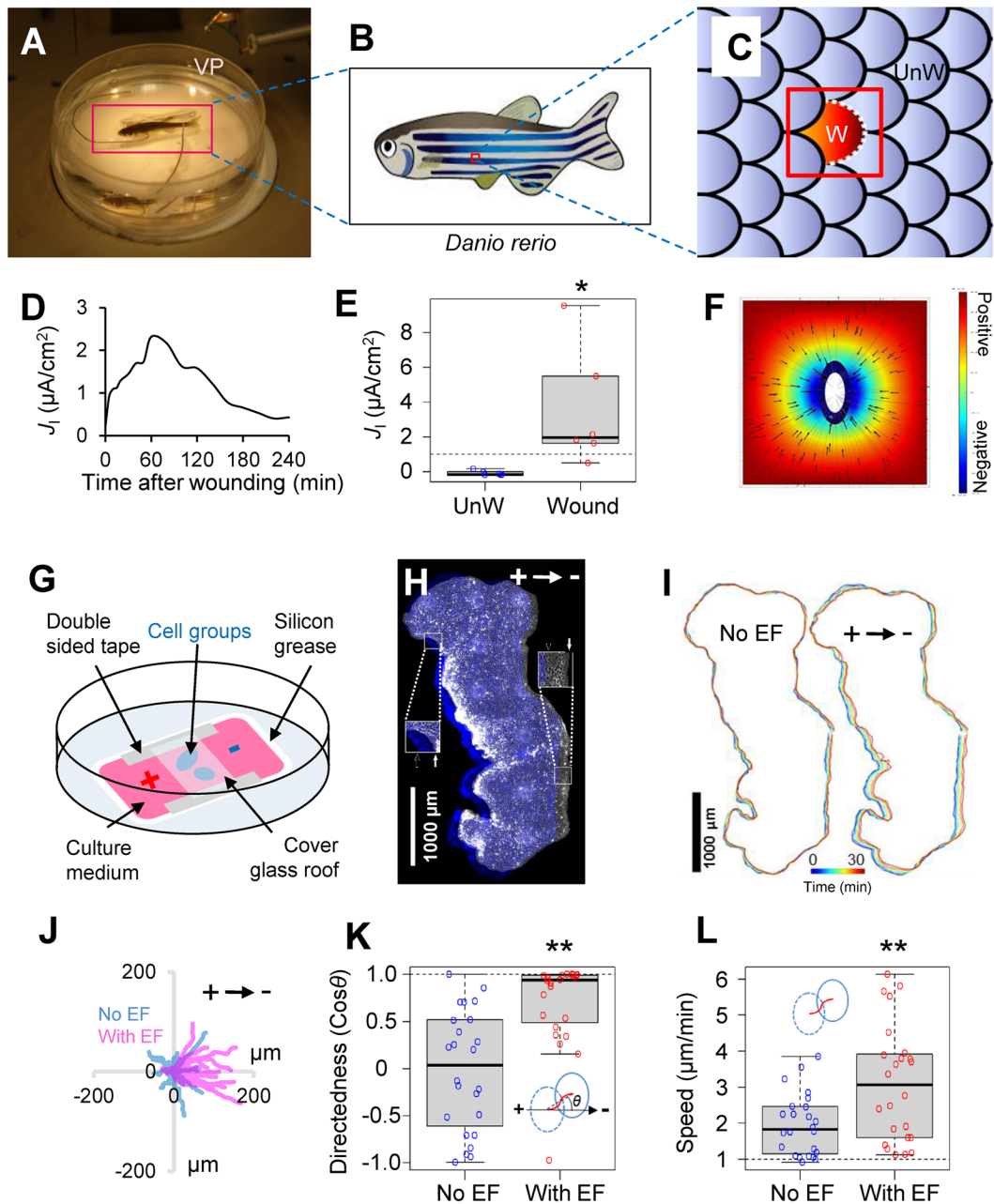
FIGURE 1: Physiological EF drives epidermal cell groups to the cathode. (A) Experimental setup to define bioelectrical field strength of scale wound–generated EFs. A vibrating probe (VP) is used to measure ionic currents around zebrafish scale wounds. (B) An individual wound was made by pulling a single scale (W). (C) Cartoon to show enlarged area in B. An adjacent scale is chosen as an unwound control (UnW). (D) Time lapse of a typical measurement of outward current up to 4 h after wounding. (E) Significant peak of outward electric current in scale wounds ($n = 6$) in comparison with unwounded scales ($n = 6$). *$p < 0.05$ by Student's t test. (F) Computational simulation of electric potential based on ionic current measurements in a zebrafish scale wound as depicted in C. The EF direction is oriented to the center of the wound (arrows). Color-coded scale in arbitrary units. (G) Schematic view of the electrotaxis chamber and the setup for EF application. (H) Stitched phase contrast image of a large keratocyte group at the onset (blue) and after 30 min (gray) of the EF application in the indicated orientation. Inserts represent 2× magnification of checked cathodal/anodal edge areas. Arrows mark group's boundaries before (open arrow) and after (solid arrow) EF application. This group contains approximately 13,600 cells. Scale bar, 1000 μm. (I) Group's contour overlay before and after EF application, each for 30 min in a 5 min interval. Contours are color coded as shown in the color bar. Scale bar, 1000 μm. (J) Trajectories of keratocyte groups' centroids ($n = 17$ for each condition). Duration: 30 min with (red) or without (blue) EF. Arrow indicates EF orientation. (K) Quantification of group directionality with ($n = 24$) or without ($n = 24$) EF (2 V/cm) application. Group migration (dash-lined and blue-lined eclipses) was tracked by monitoring centroid movement of each keratocyte group (red line). Directionality was calculated as cosθ. θ is the angle between the applied EF vector and vector (dashed line) connecting the first and last centroids of a group. **$p < 0.01$ by Student's t test. (L) Quantification of group migration speed with ($n = 24$) or without ($n = 24$) EF (2 V/cm) application. Migration speed is calculated as the arc length of the trajectory (red curve) divided by the time. **$p < 0.01$ by Student's t test.

We then applied an external EF of strength comparable to what was measured in vivo (Figure 1G and Supplemental Figure S1F). Time-lapse images of overlapped multifields covering the whole keratocyte group were recorded, stitched, and analyzed (Supplemental Figure S1, G and H, and *Materials and Methods*). In the absence of EFs, we observed slow migrations in a random direction (Figure 1J). When the EF was switched on, the same group exhibited a faster and directional migration as a cohort toward the cathode (Figure 1, H and I, and Supplemental Movie S1).

To assess the global migratory behavior, we tracked the centroid trajectory of each keratocyte group to determine its directionality and speed (Figure 1J). The directedness is defined as the cosine of the angle between the centroid displacement vector and the EF vector (Figure 1K). Compared to the random migration in the no-EF group (directedness equal to 0.022 ± 0.129, $n = 24$), applying an EF (2 V/cm) induced a robust directional migration of the keratocyte group to the cathode (directedness equal to 0.707 ± 0.093, $n = 24$) (Figure 1K). Besides the significant directional difference, the trajectory speed in EF (3.100 ± 0.330 μm/min, $n = 24$) was significantly faster than that for groups in no-EF control (1.955 ± 0.173 μm/min, $n = 24$) (Figure 1L). The group's migration became directional in a voltage as small as 1 V/cm (Supplemental Figure S2A). The directed migration of keratocyte groups to the cathode was voltage dependent: a significant speed increase was observed when the applied EF was equal to or larger than 2 V/cm (Supplemental Figure S2B). Altogether, the data suggest that external EFs of physiological strength guide migration of large keratocyte groups and allow investigation of collective cell motility initiation (Travis, 2011).

EF induces front-to-rear motility gradient in epidermal cell groups

Whole keratocyte groups initiated directed migration in EFs, but how do different group regions behave in response to EFs? To address this question, we used the particle image velocimetry (PIV) technique (Thielicke and Stamhuis, 2014) (Supplemental Figure S1H). Without EFs, velocity vectors of low magnitude (from 0 to 0.55 μm/min), directed radially outward, are distributed throughout the group (Figure 2A, bottom left), suggesting a slow expansion of the group.

There were significant differences in movements along and perpendicular to EF, and so we break the velocity vectors into two components, u and v, which are the velocity components along and perpendicular to EF, respectively (see *Materials and Methods*). For brevity, we will call u- and v-components of the velocity simply u- and v-velocity, respectively. In what follows, we call the side of the group facing anode the rear, the side of the group facing cathode the front, and the group edges in the directions perpendicular to EF the group sides.

By mapping u-velocities (Figure 2A, middle left) and v-velocities (Supplemental Figure S3A, left), we confirmed the slow expansion of the group before the EF is on (see also Supplemental Movies S2 and S3). In contrast, applying an EF induced a u-velocity gradient from the rear to the front with the highest velocity (7.24 μm/min) at the front (Figure 2A, right). The EF application caused a significant fourfold velocity increase at the front compared with no EF control (Supplemental Figure S3E). Comparing u- and v-velocities, we found that the velocity increase was essentially due to the increase of the u-velocity (Supplemental Figure S3C). Meanwhile, the mean v-velocity had a small, yet significant reduction in magnitude compared with that of the no-EF control (Supplemental Figure S3D). Note that the expansive v-velocity at the sides of the group without the EF switched inwardly after the EF was on (Supplemental Figure S3B), suggesting that as the group started to extend due to

the rear-to-front u-velocity gradient, cells at the sides of the group started to converge inwardly to compensate (Cohen *et al.*, 2014).

The increase in u-velocity was spatially graded: the velocity directed to the cathode increased dramatically at the group's front, while the velocity increased only moderately at the center and remained low at the rear of the group (Figure 2, A and B). The dynamics of this polarization process (Supplemental Movies S2 and S3) revealed that directionality inside the group increased very rapidly and almost simultaneously at the front and center, suggesting equal EF-sensing capabilities of all cells inside the group (Figure 2B). A short directional delay for the cells in the rear after EF application (Figure 2B) was likely due to the outward, expansive cell movements at the future rear of the group before EF application (Figure 2C): it probably takes time to reverse the cells at the prospective rear. The velocity of the cells increased more slowly (Figure 2C) than directionality. Cells in the rear facing the anode experienced a more pronounced time delay before reaching their speed maxima (Figure 2C). Analysis of several groups revealed similar directionality and velocity patterns (Supplemental Figures S4 and S5).

To support the PIV analysis, we manually tracked centroids of many cells from the rear, center, and front regions of the group (Supplemental Figure S1H). In the absence of the EF, cells in the right and left (future front and rear, respectively) regions of the group (less than 100 μm from boundaries) underwent outward movement, while the cells in the central region moved very little (Figure 2D, left). The migratory velocity everywhere was small, with a displacement of less than 50 μm after 30 min (Figure 2D, left). In contrast, when the EF was switched on, cells at the front accelerated dramatically, undergoing a directed migration to the cathode with the longest displacement up to 250 μm during EF exposure for 35 min (Figure 2D, right). Cells in the central region were also performing accelerated cathode-oriented migration, with an average displacement close to 100 μm (Figure 2D, right). Cells in the rear notably shifted from the anode-directed to the cathode-directed motility, with a small displacement of less than 50 μm (Figure 2D, bottom).

Then, we analyzed the directionality of each group of cells. As the EF was switched on, the cells at the front that were already biased to the cathode, very rapidly (within 5–6 min) increased their cathodal directedness to 1 (Figure 2E). The previously unbiased cells from the central region reacted almost without a delay (lagging the front cells by 2–3 min) and increased their cathodal directedness to 1 within ~5 min after the short lag (Figure 2E). The cells at the rear that were moving to the anode before the EF exposure experienced a longer lagging time (up to 10 min), after which they turned to cathode with the turning rate similar to that of the cells in other regions (Figure 2E).

Because the migration velocity difference between the front and rear of the group increased dramatically after EF application, the group stretched in the EF direction (Supplemental Movie S2), and one would imagine that the cell–cell contacts could be disrupted. This was indeed the case. We noticed multiple holes formed inside large groups in EFs, which could be identified in time-lapse images (Supplemental Movies S2 and S4). Holes developed only during EF application and grew at a rate compatible with the EF-induced u-velocity at the onset of hole formation. Holes emerged as early as 15 min after EF application (Supplemental Figure S6A), and their diameters increased progressively (Supplemental Movie S4). To quantify the dynamic change of the holes, we monitored the area of the holes with respect to that of the group after EF application. At the end time point, after an EF was applied for 45 min, the total area of the holes reached 6.4% of the tissue size (Supplemental Figure S6B), with the largest holes measuring up to 3% of the group size
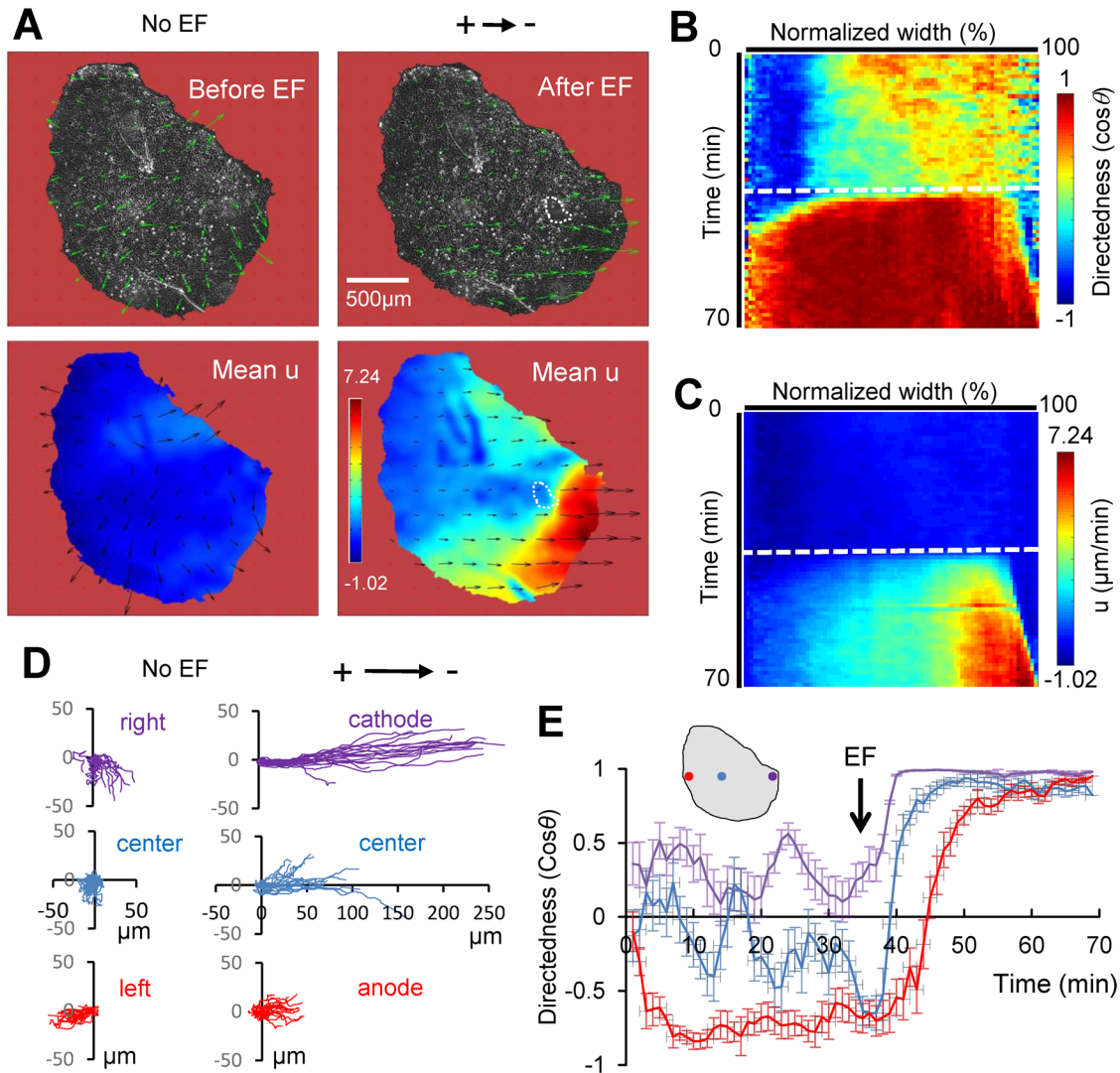
FIGURE 2: EF induces a distinct front-to-rear polarization pattern, resulting in regional migratory behavior. (A) PIV analysis of a representative keratocyte group (of approximately 7600 keratocytes) before (left panel) and after (right panel) EF application. Top row shows velocity vectors overlaid on phase contrast image; in the bottom row, color-coded, time-averaged components of velocity parallel to EF are shown (in µm/min, for EF of 2 V/cm). Scale bar, 500 µm. Note the increased alignment and magnitude of the velocity vectors, as well as regional front-to-rear differences induced by EF. White dashed enclosure highlights a hole in the group that was induced by EF. (B) Color-coded kymograph of directionality (cosθ). Vertical dimension is time in minutes, and horizontal dimension is projected mean directionality (cosθ) spanning the whole width of the keratocyte group; the EF oriented to the right. Dashed line indicates when EF (2 V/cm) is on. (C) Color-coded kymograph of the u-component (parallel to the EF) velocity in µm/min. Vertical dimension is time in minutes, and horizontal dimension is the projected time-averaged u-velocity spanning the whole width of the group. (D) Manually tracked cell trajectories in three regions (left, center, right) (n = 20 for each color-coded region) of the group before and after EF (2 V/cm in the indicated direction) application. Distances are in µm, and duration is 35 min. (E) Dynamics of mean directedness (cosθ) of the tracked regional cells. Directedness is calculated at 5 min intervals from a representative group in at least three repeated experiments. Error bars are SE for n = 20 regional cells. Color codes are the same as in D (positions are approximate). Arrow indicates when EF was switched on.

(Supplemental Figure S6C). Interestingly, holes appeared to form right where the u-velocity gradients were maximal (Figure 2A and Supplemental Figure S6D). The cells at the hole edges did not display lamellipodia protruding into the holes; instead, the hole edge appeared to be contractile (Supplemental Figure S7).

Inhibiting PI3Ks changes the rear-to-front velocity gradient in groups migrating to the cathode

Individual cells use competing signaling networks to transduce external electrical signals into cytoskeletal biases (Allen *et al.*, 2013;

Sun *et al.*, 2013). One such signaling network is the so-called "frontness" "Gβ-PI3K-Actin" pathway (Trepat *et al.*, 2012; Shellard and Mayor, 2019). It has been demonstrated that during directed migration under either chemoattractant gradient or electrical guidance, PI3K is recruited to the plasma membrane at the front areas of migrating cells activating PIP3 (Parent *et al.*, 1998; Zhao *et al.*, 2006). PI3K influences cell guidance through its interaction with small GTPases and actin; the mechanism of these interactions and the resultant role of PI3K in regulating directed migration are still under investigation. Given that inhibition of PI3K reversed individual

keratocytes to the anode (Sun *et al.*, 2013), we were curious what effect PI3K has on the collective motility initiation. Thus, we used the pharmacological inhibitor of PI3K, the LY294002 compound at the widely used working concentration of 50 μM (Vlahos *et al.*, 1994), in combination with EF application. We confirmed that this PI3K inhibition globally reduces PIP3 in the cell group (Supplemental Figure S8). For brevity, below we call the PI3K-inhibited cell groups treated with the LY compound "LY" groups, and we call untreated groups "Ctrl" groups.

After an EF was applied to the LY group, motility was initiated to the cathode (Figure 3). Interestingly, the speeds of the cells at the rear and center of the group were greater than that at the front (Supplemental Figure S9A and Supplemental Movie S5), in contrast to the velocity gradient in the Ctrl group. This reversed velocity gradient was also captured by PIV analysis (Figure 3, A–C, Supplemental Figure S9, B and C, and Supplemental Movie S6). Similar patterns were also observed in other LY groups (Supplemental Figures S10 and S11). Tracking individual cells within the group in response to an EF and in the presence of LY also confirmed this spatial pattern (Figure 3F). Interestingly, cells from different regions of the group increased their directionality in synchrony, achieving the maximal directedness in about 5 min (Figure 3G). This again suggests that all cells in the group sense the EF signal individually and independently.

Two additional observations are worth noting. First, from comparing the directedness and velocity kymographs in the Ctrl and LY groups (Figure 2B and Supplemental Figure S4A vs. Supplemental Figure S9B, respectively), it is apparent that in LY groups there was no significant radial expansion of the group as in Ctrl groups (see potential explanation in the *Discussion*). This likely explains why all cells within the LY group initiate motility in sync (the cells were not moving vigorously before the EF was applied), while in the Ctrl group there are regional time delays (the cells at the future front were already moving in the "correct" direction, while the cells at the future rear had to turn around). Second, because in LY groups the rear was faster than the front, these groups are expected not to extend as they move in the EF, but to converge (Supplemental Movie S5), so no emerging holes are expected. Indeed, we observed no holes in any of the LY groups in the EF.

PI3K is known to be required for strong spatially coordinated protrusion in single cells (Yoo *et al.*, 2010; Shellard *et al.*, 2018). To test whether another perturbation of cell protrusion will result in the same effect on galvanotaxis as PI3K inhibition, we used small molecule CK666 to inhibit the Arp2/3 complex responsible for dynamic branched-actin protrusive structures in motile cells (Henson *et al.*, 2015). For brevity, below we call the Arp2/3-inhibited cell groups treated with CK666 "CK" groups. We found, indeed, that the regional motility distributions in the CK groups are like those in the LY groups (Figure 3, Supplemental Figures S12 and S13, and Supplemental Movie S7): the velocity gradient across the CK group reveals cathode-directed motility with velocity decreasing from the anodal rear to the cathodal front.

Myosin-dependent activity is essential for cohesiveness and is required for collective EF-induced directionality and turning

Myosin activity is crucial for the polarization and motility initiation of individual keratocytes (Yam *et al.*, 2007; Barnhart *et al.*, 2015) and is a dominant factor in controlling EF-directed migration of cytoplasmic fragments (Sun *et al.*, 2013). Thus, we hypothesized that the myosin activity played an important role in collective directional response to EF and treated cell groups with 50 μM blebbistatin (BB),

an inhibitor of myosin-mediated contractility (Kovacs *et al.*, 2004). Below, for brevity we call the groups treated with blebbistatin "BB" groups. However, upon inhibition of myosin, cohesiveness between the individual cells in the groups was weakened, likely because myosin-powered contraction is necessary for stabilizing cell–cell adhesions (Efimova and Svitkina, 2018). Consequently, a fraction of the cells dissociated from the group's periphery during galvanotaxis (Supplemental Movie S8), as has been reported previously (Rapanan *et al.*, 2014). Although this prevented us from characterizing regional cell behavior by PIV analysis, we were able to track individual cells in various regions and assess the critical roles of myosin during EF-manipulated turning in this epidermal cell group model.

Total disruption of myosin activity can affect the ability of individual cells to migrate efficiently regardless of the presence or absence of an EF. To test whether a more direct disruption of cell–cell adhesion produces an effect similar to that of the loss of myosin activity, we used the helating agent EGTA to disrupt cell–cell adhesions (Worley *et al.*, 2015). In the EGTA-treated groups, cells dissociated from each other (Supplemental Movie S9). Tracking individual cells after EGTA treatment (Supplemental Movie S9 and Supplemental Figure S14) showed that the dissociated cells do undergo biased directional migration to the cathode after EF is switched on, but the migration is much more random and imperfect compared with the collective cohesive migration. This suggests that integration of the cells into a collective through mechanical coupling confers additional abilities to quickly affect the directionality of cell movement at the tissue scale compared with individual cells.

We showed earlier that individual keratocytes respond to reversal of a preexisting EF by making U-turns (Sun *et al.*, 2013). A recent study reported that cells in a cultured Madin–Darby canine kidney (MDCK)-II monolayer could also make local U-turns when manipulated by turning the EF (Cohen *et al.*, 2014). To assess whether keratocyte groups can follow EF direction collectively, we used the sequence of No EF, EF to the right, EF to the left, and EF off conditions, each 30 min long (Figure 4A). We then monitored the migration trajectories of individual cells from different regions of a large keratocyte group (Figure 4B and Supplemental Movie S10). We observed the characteristic U-turn trajectories in all regions of the group (Figure 4C and Supplemental Movies S10 and S11). This confirmed that cohesive cells maintain the competence to change motility direction in response to electrical guidance cues.

We found that in BB groups, cells were largely unable to develop coherent EF-induced directionality: Figure 4C (right column) and Figure 4D (bottom) revealed that the partly disjointed cells from the left of the group continued their leftward ("incorrect") movement during the 30–60 min interval when the cathode was at the right. Meanwhile the rightward movement of the cells from the cathodal side of the group, which were already biased to the right in the beginning, decreased their cathodal bias when the EF was on. Curiously, cells from the center of the BB group exhibited a somewhat slow shift to the cathode in the 30–60 min interval, likely because these cells still maintained reasonable mutual cohesiveness and could respond directionally to the EF.

Inhibition of PI3K did not abolish the ability of individual cells in any region of LY groups to make EF-steered U-turns (Figure 4, C and D, and Supplemental Movie S12). In contrast, cells in BB groups did not exhibit coherent directional movements or turns when the EF was reversed during the 60–90 min interval (Figure 4, C and D, and Supplemental Movie S13). Curiously, the cells at the left margin of the BB group started to shift to the right (in the "wrong" direction, to the anode) during this time interval, which is likely the result of the partial cohesiveness between cells: by that time, the center and
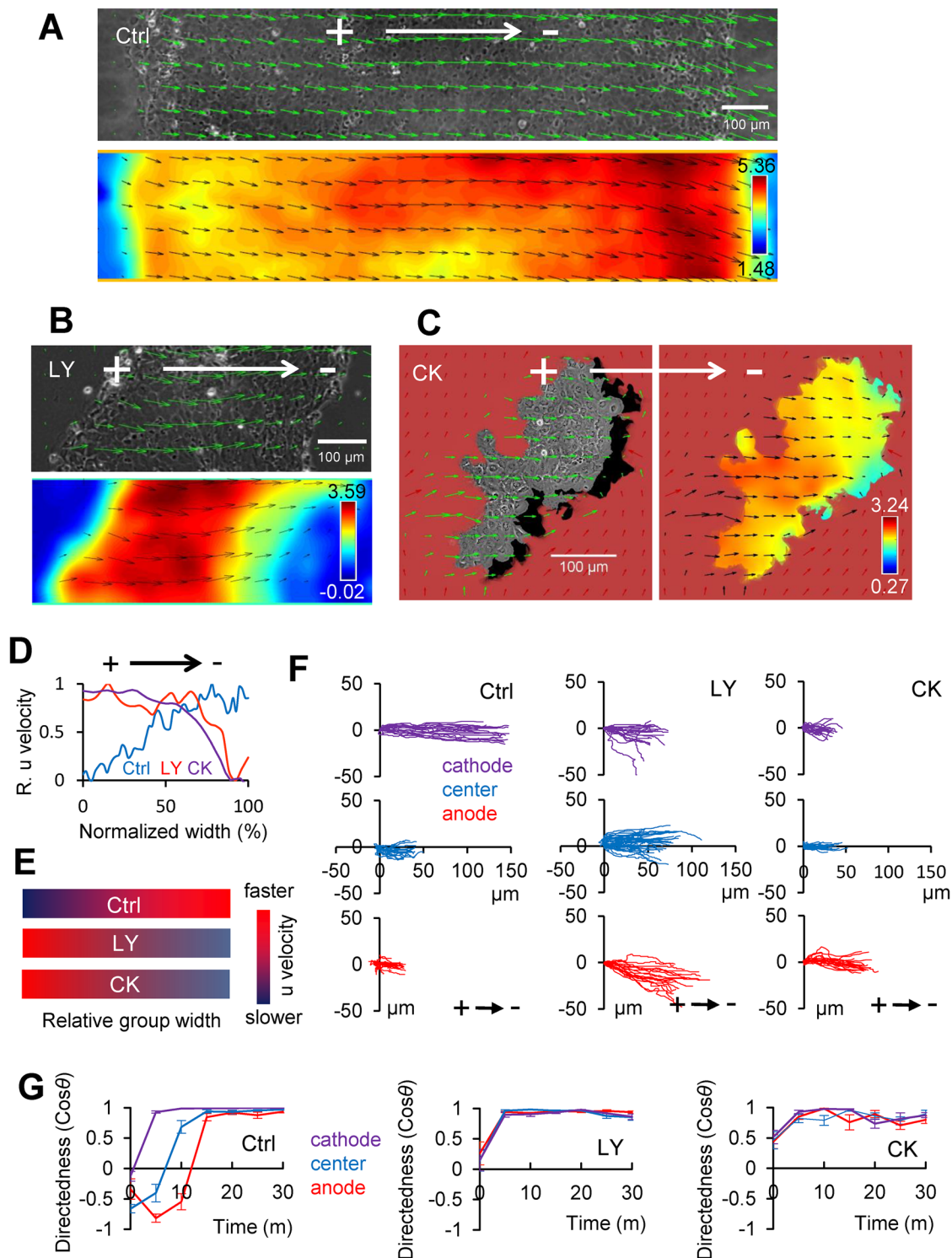
FIGURE 3: Inhibition of PI3K and Arp2/3 complex does not change cathodal motility of the whole group but reverses the velocity gradient within the group. (A) PIV maps of keratocyte groups in the absence (Ctrl) or (B) presence of 50 μM LY294002 compound (LY) or (C) CK666 (CK). Velocity vectors are overlaid on the phase contrast image of a slice of the group at the initial point or color-coded u-velocity map after 30 min of EF exposure (2 V/cm in the indicated direction). Scale bar, 100 μm. (D) Line scan of u-velocity (normalized from minimum [0] to maximum [1]) spanning groups in parallel to EF (the distance across the group's width is normalized from 0 at the anode to 1 at the cathodal side). Note the reversed front-to-rear velocity gradient in the presence of LY or CK compared with that of the Ctrl. (E) Schematic summary of the velocity gradients in these three cases. (F) Manually tracked cell trajectories from the anodal, cathodal, and central regions. Each line represents an individual keratocyte ($n = 20$ from each color-coded zone) over a 30 min time course of EF application (2 V/cm in the indicated direction). Distances are in μm. (G) Dynamics of mean directedness (cosθ) of cells in three regions of Ctrl, LY, and CK groups under EF application (2 V/cm). Directedness is calculated from a representative group in at least three repeated experiments. Error bars are SE across for $n = 20$ regional cells.
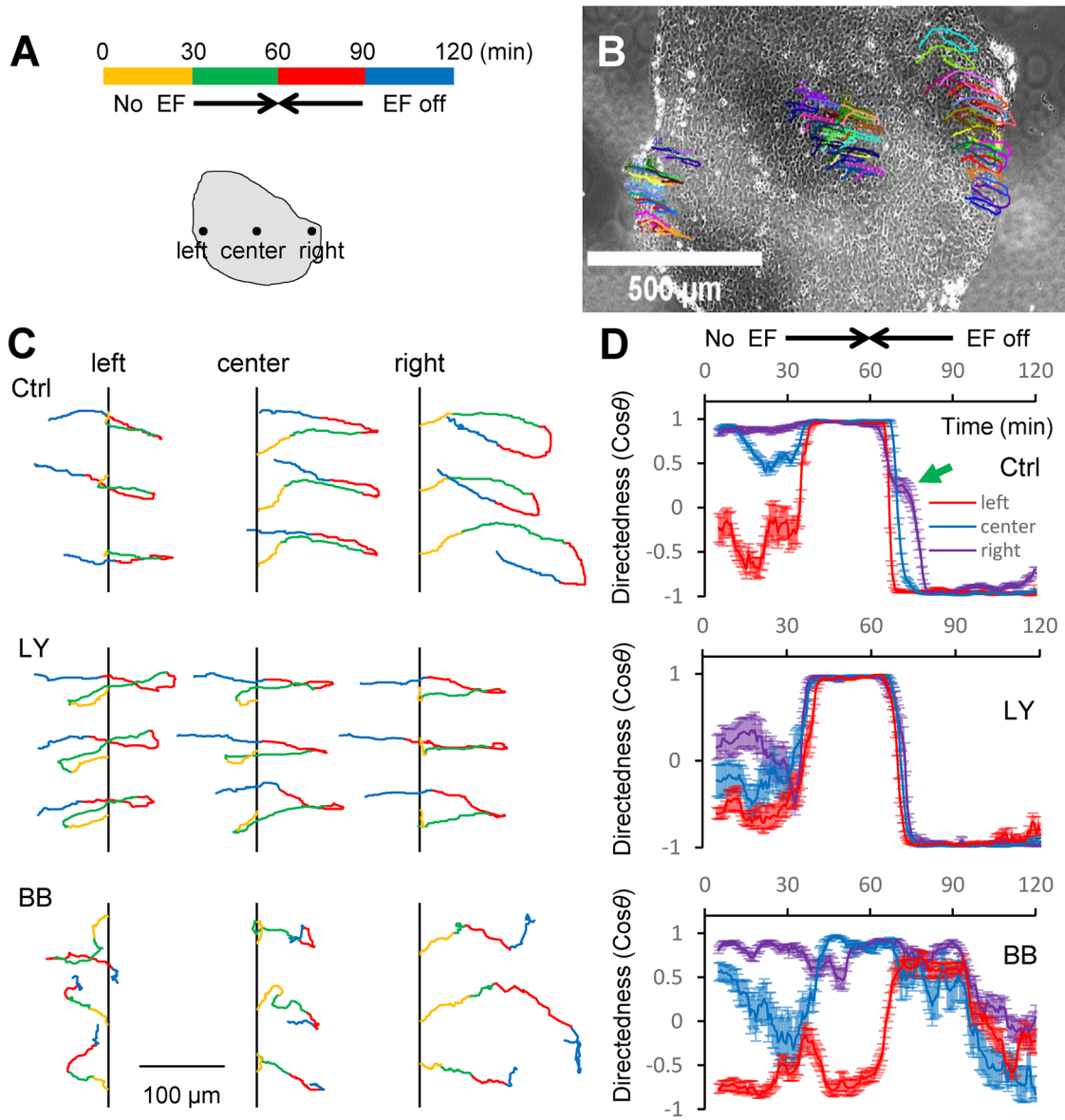
FIGURE 4: Myosin is necessary for collective EF sensing and EF-induced U-turns. (A) Color-coded time sequence of No EF, EF (2 V/cm) to the right, EF (2 V/cm) to the left, and EF off in 30 min intervals. Schematic below the time sequence shows three regions at the left, center, and right of the group from which cells are tracked. (B) U-turn tracks overlaid on the phase contrast image of the cell group. Each curve represents an individual cell trajectory. Arbitrary different colors are used to distinguish trajectories more easily. See also Supplemental Movies S8–S11. (C) Three randomly chosen cell trajectories are shown from each of the three regions of the group marked in A for each of the three chemical conditions—in the absence (Ctrl) or presence of 50 μM PI3K inhibitor LY294002 (LY) or myosin phosphorylation inhibitor BB. For visual clarity, in each set of three trajectories, the initial x-coordinate is shifted to the same vertical line while the initial y-coordinate is shifted to sufficiently separate the trajectories. The color coding along the trajectories is the same as in A to better visualize the directions in which the cells are moving during each of the four EF time intervals. Scale bar, 100 μm. (D) Dynamics of mean directedness (cosθ) of regional cells (color codes and timescale apply to all three plots). Directedness is calculated in 5 min intervals of representative groups in at least two repeated experiments in each condition. Error bars are SEs for n regional cells (n between 15 and 20) for each region. The green arrow points to delayed directional response of former "leader"/new "trailer" cells in Ctrl.

right parts of the BB group diverged so far to the right from oppositely moving cells at the left margin that this greater center/right part of the group pulled the cells at the left with it.

Note that in the Ctrl group the cells leading the group during the 30–60 min interval respond to the EF reversal by starting to decrease their directedness value slightly sooner than the cells from the center and rear (Figure 4D). However, after the head start, these

formerly leading cells took a much longer time to finish the turn (Figure 4D, green arrow), indicating that these cells were more "directionally inertial" than others. Also, note that what we call a U-turn could in fact represent two types of behavior: a smooth and wide turn led by persistent lamellipodium, or a repolarization—disappearance of one lamellipodium and emergence of another one in a new direction. The smooth U-turn is normally associated with a

smooth and wide trajectory, the repolarization with a sharp turn and retracing of the previous path (Sun *et al.*, 2013). It is apparent from Figure 4C that in the Ctrl group the formerly leading cells make a smooth U-turn, while all other cells (as well as cells from all regions in the LY group) undergo repolarization.

We quantified the regional turning and motile behaviors in Ctrl and LY groups by measuring the displacements that the cells made during the EF-guided 30–60 and 60–90 min intervals and the time moments when cells reversed their directionalities (Supplemental Figure S15A). This quantitation revealed that despite statistically significant 2–3 min regional differences in turning times, these moments were remarkably similar in all regions of the LY group and at the center and former rear of Ctrl group (Supplemental Figure S15B). Importantly, there was little difference between turning times in the centers of the Ctrl and the LY group. All these turning times were in the approximately 5–8 min range (starting from 60 min at which the EF was switched). These repolarization times were essentially the same as the initial polarization times (Figures 2 and 3). The only exception was the extra time necessary for the former leading cells of the Ctrl group to make their U-turn (Supplemental Figure S15B). Also, comparison of the displacements made during the EF-guided 30–60 and 60–90 min intervals (Supplemental Figure S15, C and D) revealed that, after turning, the velocity gradient in the Ctrl group was maintained—the new leader cells moved faster than the new trailing cells during the 60–90 min interval. Curiously, the velocity gradient in the LY group disappeared—the new leaders did not move slower than the center/trailing cells during the 60–90 min interval, as they did in the previous time interval. Finally, note that despite the apparently smaller displacements over the 60–90 min interval compared with those during the 30–60 min time interval, the cell speeds after reversal are like those before the reversal. This is explained by the geometry of displacements (Supplemental Figure S15A) and time delays: after the turn, cells must spend time to reach the point where they were at the 60 min mark, and only then does the net displacement start increasing, while before the turn cells have a longer time to build up their displacements.

Ctrl and LY groups continue to move directionally after the EF is switched off

Interestingly, the EF-induced directionality of the Ctrl and LY groups was maintained after the EF was switched off (Figure 4D), indicating that after the EF signal polarizes the groups and initiates their motility, the groups collectively maintain their polarized state and migrate in the absence of an EF. We have not explored how long the EF must be on for this stabilizing effect, but a much shorter EF application for several minutes did not switch the groups into the stable motile state.

DISCUSSION

To summarize, we found that applying physiological-level EFs to large groups of primary epidermal keratocytes derived from zebrafish scales initiated a group's migration to the cathode in minutes, whether PI3K was inhibited or not. Though both large uninhibited and PI3K-inhibited groups move to the cathode, the cell speed distribution in these groups was different: cell speed reached maximum at the front of the uninhibited groups, but at the front of the PI3K-inhibited groups cell speed was minimal. In agreement with Cohen *et al.* (2014) and Cho *et al.* (2018), the groups were able to repolarize and change direction in minutes upon the EF orientation reversal, as well as to maintain stable directional motility when the EF was switched off after 30 min of the EF-induced migration.

Roles of PI3K and myosin in collective galvanotaxis

PI3K is the key part of important pathways relaying extracellular signals to actin networks at the cell leading edge in several cell types (Zhao *et al.*, 2006; Kolsch *et al.*, 2008; Meng *et al.*, 2011). A related recent study reports that PI3K is up-regulated in leader cells and that when PI3K is inhibited, collective migration of MDCK epithelial cells is disrupted (Yamaguchi *et al.*, 2015). Our study shows that when PI3K is inhibited, the peripheral cells in the group with large lamellipodia were affected the most and the dominant number of inner cells, which seem to be PI3K independent, are sufficient to make the whole group directional in response to EFs (see below). This is in line with the results in Cohen *et al.* (2014), where confinement of leading cells against a physical barrier renders them unable to extend lamellipodia, thus phenocopying PI3K inhibition and shifting the regulation of collective behavior to the bulk of the cell sheet that now responds to EFs by increasing contractile forces in the posterior-most cells.

While loosening a tissue may help initiate EF-guided cell migration as demonstrated recently (Shim *et al.*, 2021), in general, reducing tissue integrity likely has adverse effects and may reduce the efficacy of collective cell migration (Li *et al.*, 2012). Indeed, we observed that when myosin was inhibited, cohesion within the group was partially lost (relevant mechanisms were discussed in Vedula *et al.*, 2014, and Hirata *et al.*, 2015), and the group's ability to polarize collectively and to follow EF guidance was impaired. A similar result was produced upon disruption of cell–cell adhesion directly with the calcium chelator EGTA. As a result, multiple cells moved erratically and collided with each other often, and these random collisions and movements were likely to override the biasing effect of the EF. To conclude, myosin is required for collective cell directional response to EF, but PI3K is dispensable, suggesting that the primary role of EFs in guiding collective migration is the orientation of contractile forces along the EF direction, rather than induction of leading cell lamellipodia formation.

Qualitative model of collective cell motility initiation induced by EFs (Figure 5)

We propose that cells within large groups sense EFs individually and independently. The following observations support this conclusion: First, the threshold EF at which groups sense the EF (1–2 V/cm) (Supplemental Figure S2) is the same as that for single cells (Sun *et al.*, 2018). Second, in all regions of the large group, directionality arises almost simultaneously, as is clear for LY groups. Third, collective motility initiation takes 5–10 min in EFs, the same time it takes single cells to polarize in EFs (Sun *et al.*, 2018).

We posit that the velocity gradient across the Ctrl group is the effect of the cells at the periphery of the group that have large, partially stabilized lamellipodia protruding outward, which are clearly seen in the Supplemental movies and in a previous study (Rapanan *et al.*, 2014). It is natural to assume that the rear and sides of these cells do not protrude due to contact inhibition of locomotion (Abercrombie and Heaysman, 1953; Mayor and Carmona-Fontaine, 2010) and that these cells are strongly polarized outward. This is the reason the groups are expanding before EF application: the peripheral cells crawl slowly outward, stretching and expanding the group. After the EF is applied, peripheral cells on the group's cathodal side can move to the cathode much faster than the inner cells because of their large stabilized lamellipodia. These peripheral lamellipodia could also be responsible for slowing trailer cells on the anodal side of Ctrl groups, pulling trailer cells in the anodal direction and enhancing the rear-to-front velocity gradient. This is consistent with our observations of both PI3K- and Arp2/3-inhibited cell groups,
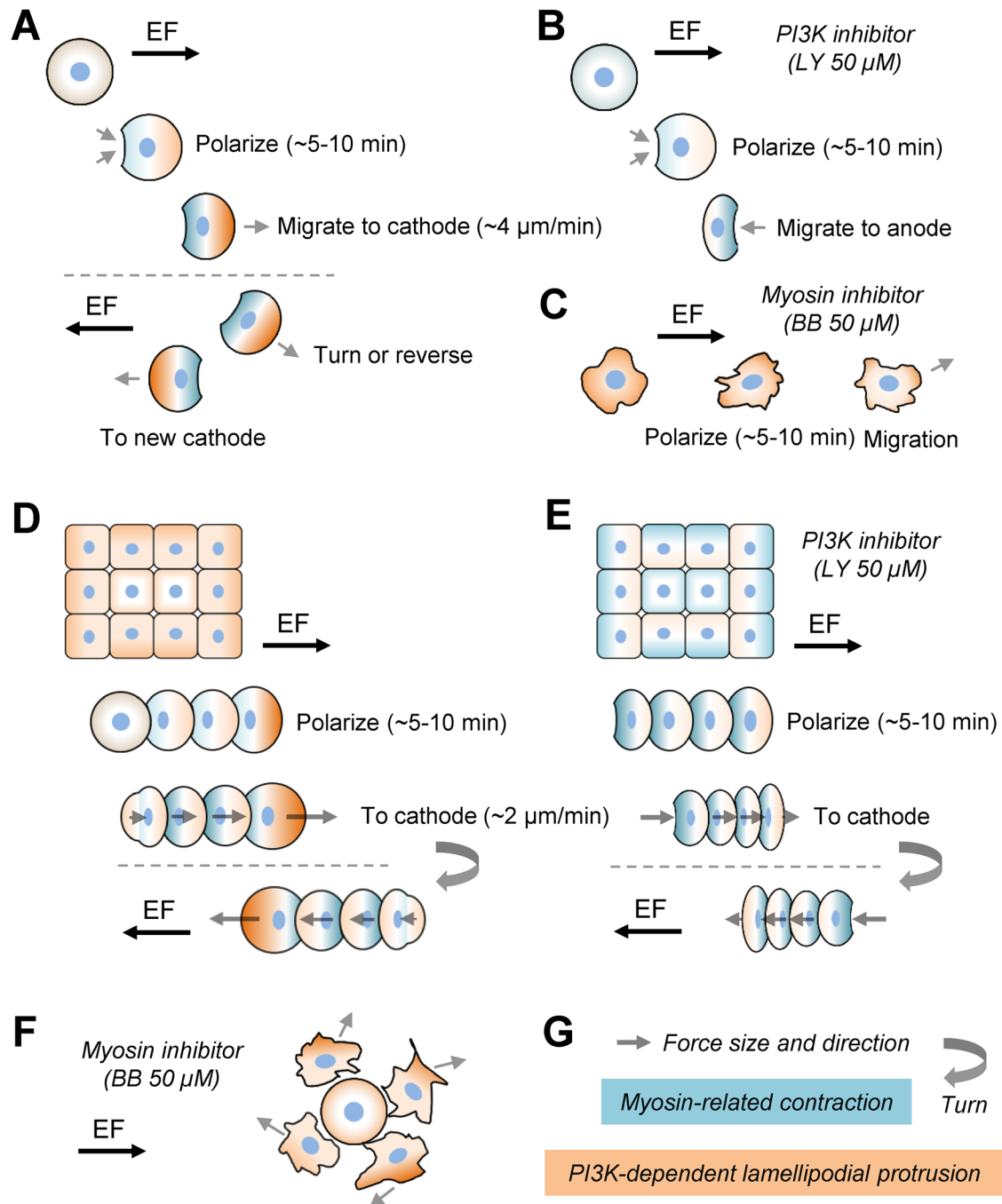
FIGURE 5: Qualitative model of collective EF-induced cell polarization and motility. (A) EF polarizes symmetric stationary single cell from the rear in minutes; a myosin/contraction, protrusion-independent, mechanism driving retraction of the future rear is responsible for the polarization. After the initial polarization, the robust lamellipodial protrusion starts and guides the rapidly moving cell to the cathode. The cell responds to EF reversal by a U-turn or repolarization to go to the new cathode. (B) When PI3K is inhibited, the initial polarization is the same because PI3K does not affect the myosin/contraction, protrusion-independent, mechanism. (C) When myosin is inhibited, EF can still polarize the cell, but the resulting motility and cell shape are relatively random and unsteady. (D, E) Inside the cohesive group, cells sense EF individually, polarizing in minutes much like single cells. We hypothesize that individual cells polarize from the rear and that the myosin/contraction mechanism is dominant for both initial polarization and stable motility. The only significant difference between the control and PI3K-inhibited groups is that protrusions in the leading and trailing cells in the former accelerate the front and slow the rear, while in the latter the regional differences in the group are muted. (F) When myosin is inhibited, the cells lose mutual cohesion. The combined effects of randomized motility of individual cells and frequent collisions with neighbors, resulting in transient contact inhibition of locomotion and pulling on each other, override the guiding effect of EF. (G) Keys for the notations.

where cells at the group rear can move to the cathode without a delay.

These arguments could also explain the velocity distribution across the LY group; PI3K is required for strong spatially coordinated protrusion in single cells (Yoo *et al.*, 2010; Shellard *et al.*, 2018), and so weakly protruding peripheral cells on the cathodal side of LY groups could be inherently slower than inner cells in these groups, slowing the group's front. Meanwhile, weakly protruding peripheral cells on the anodal side of these groups do not slow the inner cells near the group's rear, contributing for the characteristic faster rear/center and slower front velocity gradient.

Interestingly, both single PI3K-inhibited cells and cohesive groups of such cells polarize to the cathode. This is suggestive of a myosin-dependent and PI3K-independent, EF-sensitive polarization mechanism. In single PI3K-inhibited cells, larger lamellipodia eventually reorient the cells to the anode after the cell is polarized, but in cohesive groups the lamellipodia are likely cryptic (Farooqui and Fenteany, 2005). Lamellipodia of these cells are suppressed by physical coupling to neighboring cells on all sides (Cho *et al.*, 2018), and also intercellular adhesions and signaling pathways (Li *et al.*, 2012; Etienne-Manneville, 2014) are organized differently in inner and edge cells. Owing to these different organizations of cytoskeletal and signaling networks inside the group and at its edge, it is possible that the balance of the signal transduction pathways (Sato *et al.*, 2009; Sun *et al.*, 2013) in inner cells differs from that in single and edge cells.

Our data show that in groups where PI3K or Arp2/3 are inhibited, velocities of cell movement become reversed compared with controls, that is, the cells in the group rear move toward the cathode with greater velocity than cells in the group front. This behavior may be explained by the differential recruitment of actomyosin machinery to the free edges of the peripheral cells before EF application. In this scenario, cells at the group front would have their contractile machinery localized to the free edge, causing them to remain in place when the EF is applied and allowing the cells in the group rear, which is already polarized toward the cathode, to compress the tissue along the EF axis. Fitting with this hypothesis, the cells at the front of the Arp2/3-inhibited cell groups show decreased or in some cases low levels of movement toward the anode.

In general, our results suggest that inner cell groups are polarized differently from peripheral cells, also observed in Rapanan *et al.* (2014), where the authors show an unpolarized myosin distribution in keratocytes inside the cell sheet. Additional evidence for these different polarities is provided by our observation that cells at the periphery of tears formed during cell sheet migration do not extend lamellipodia into the newly available front but instead appear to reinforce the edges of the tears with additional actin fibers, suggesting that inner cells may have robust inhibition of protrusive activity, at least at the timescales of the experiments here.

Other potential models

First, the "leader" cell theory has earned much popularity (Omelchenko *et al.*, 2003; Poujade *et al.*, 2007; Khalil and Friedl, 2010; Yamaguchi *et al.*, 2015): peripheral cells, which often have large protrusive appendages extending outward and unobstructed by contact inhibition from neighboring cells, sense extracellular signals and develop dominant active propulsion, while the inner cells polarize in response and follow the leaders. Our observations of PI3K-inhibited groups argue against this possibility: in those groups, the cells at the center and rear of the groups appear to push forward the cells at the group's front.

Second, Cohen *et al.* (2014) observed that cells at the boundary of epithelial cell groups migrating in EFs did not respond to EF directionally when the field was perpendicular to the directionality of leading cell migration, implying that the inner cells, instead of the peripheral cells, guide the whole groups. Similar observations were made for clusters of malignant cancer cells responding to chemical gradients (Huang *et al.*, 2009). Our observations of Ctrl groups argue against the possibility that peripheral cells passively follow inner cells: in those groups, cells at the group's front respond slightly earlier and go to the cathode faster than cells at the center and rear. This again supports the view of the cells sensing EFs individually and eventually integrating the response at the level of the group.

Finally, there is a possibility that cells inside the group are chemically and electrically integrated into a large internal supracellular structure. Integrated cytoskeletal global networks in collectively migrating keratocytes (Rapanan *et al.*, 2014) and in neural crest cell groups (Shellard *et al.*, 2018) were reported. Traction force measurements showed integrated changes in patterns of intercellular stresses that precede changes of individual cell shapes (Cho *et al.*, 2018) in the groups in EFs, indicating a supracellular response. Such integration could effectively enable the group to sense EFs globally on the length scale of the whole group. Indeed, cells can read the bioelectrical state of distant regions in the group via chemical molecules redistributed across long distances by a gradient of bioelectric cell state (Durant *et al.*, 2019). There is also a possibility of global measurement of group size and of global coordination through mechanical stresses or diffusing morphogens (Camley, 2018). This model is hard to rule out definitively; however, one would expect that a large supercell is more sensitive to weaker EFs than a single cell, which is not the case. A potential way to tease apart the two models is to compare the amount of time it takes a small cell collective to initiate posterior cell movement with that of a larger cell group, with the prediction that a signal propagated through a larger collective will take longer to reach the cells in the posterior compared with propagation through a smaller group if the groups are supracellularly integrated before EF application.

Implications for wound healing

Efforts have been made recently to use exogenous EFs to enhance cellular motility and speed up reepithelialization, thereby promoting chronic wound healing, but results have been controversial (Kloth and Zhao, 2010; Kloth, 2014; Barnes *et al.*, 2014). Groups with holes that formed due to stretching generated by velocity gradients either could indicate a mechanism of failure to reepithelialize the wound surface or could be a part of a rapid reepithelialization strategy in order to cover large wound surfaces quickly (Richardson *et al.*, 2016). Namely, even when there are not enough cells to cover the wound surface, a group with holes can establish the coverage rapidly by motility alone, and then proliferation of cells into the holes can improve the coverage.

It will also be important to learn whether chronic wounds that fail to respond to EFs have preexisting conditions resulting from compromised cellular signaling networks. Myosin is a requirement for rapid reepithelialization and subsequent wound healing in adult zebrafish (Richardson *et al.*, 2016), but PI3K action in wound healing is less clear. Recent studies showed that therapies targeting the PI3K pathway improve wound healing and attenuate tumor metastasis (Castilho *et al.*, 2013; Li *et al.*, 2013; Caino *et al.*, 2015). Another recent study showed that PI3K/Akt pathways were attenuated in the wounded skin of diabetic rats that have delayed wound healing (Lima *et al.*, 2012). We speculate that compromised PI3K signaling could lead to pathological consequences for several reasons. First,

large LY groups, though they still migrate to the cathode, are less directional (Figure 3E), while individual keratocytes are biased to the anode (Sun *et al.*, 2013), away from the wound, which could cause reepithelialization failure (Raja *et al.*, 2007). Second, the speed of the front of the LY group is slower than that in control (Figure 3E). Rapid group response to dynamic EFs (a similar observation was made in Zajdel *et al.*, 2020) could also be clinically relevant, as it is likely that the endogenous EF changes at different stages of wound healing.

MATERIALS AND METHODS
Request a protocol through *Bio-protocol*.

Measuring ionic current around zebrafish scale wounds
Adult zebrafish (*Danio rerio*, Hamilton 1822*)* strain AB were obtained from the UC Davis Zebrafish facility. All experiments were conducted in accordance with the UC Davis Institutional Animal Care and Use Committee (protocol number 16478). Single scale wound currents were measured using a modified vibrating probe technique as described previously (Reid *et al.*, 2007). Briefly, a zebrafish was immersed in a sufficient amount of fresh and clean water containing 100 mg l^{-1} MS-222 with the pH buffered by sodium bicarbonate. The anesthetized fish was transferred into a measuring container and fixed in a custom-made holder (Figure 1A). A wound was made by pulling an individual scale off a flank (Figure 1B). An insulated stainless-steel electrode, electroplated with gold and platinum, was vibrated at high frequency in solution at a reference position, far away (~2 cm) from the specimen, to establish a baseline. Under a dissecting microscope the probe, which was mounted on a three-dimensional micromanipulator, was then moved to a measurement position, approximately 50 µm above the center of the scale wound or an adjacent scale (Figure 1C). As the probe vibrates, the charge at the electrode tip oscillates in proportion to the size of the electric current. As soon as the trace becomes steady, the probe is moved slowly back to its reference position while the trace falls to baseline. Measurements were done in balanced fish Ringer's solution (NaCl 116 mM, KCl 2.9 mM, CaCl$_2$ 5 mM, HEPES 5 mM, pH 7.4), which is optimized for the fish with defined ionic composition. All the measurements were done at room temperature. The probe was calibrated at the start and end of each experiment in a known current from a constant-current calibrator unit. During calibrations and measurements, a Faraday "wall" (grounded aluminum-wrapped cardboard) covered the microscope. Data were acquired and extracted using WinWCP v4 (Strathclyde Electrophysiology Software) and analyzed using Excel (Microsoft). The scale wound–generated EF (Figure 1F) was calculated by using COMSOL Multiphysics (COMSOL).

Primary culture of keratocyte tissues
Scales were removed from the flank of anesthetized zebrafish and allowed to adhere to the bottom of EF chambers (Sun *et al.*, 2013). The scales were covered by a glass 22-mm coverslip with a stainless-steel nut on the top to hold it in position and cultured at room temperature in Leibovitz's L-15 media (Life Technologies), supplemented with 14.2 mM HEPES, pH 7.4, 10% fetal bovine serum (Invitrogen), and 1% antibiotic–antimycotic (Life Technologies). Scales were removed gently once an epithelial sheet formed (which usually took 24–48 h) (Supplemental Figure S1, A and B). The attached keratocyte cell groups (Supplemental Figure S1C) were used for drug treatment and EF application experiments. For pharmacological perturbation, drugs (all purchased from Sigma) were added in the culture medium in the following concentrations: dimethyl sulfoxide (0.1%), LY294002 (50 µM), BB (50 µM), CK666 (50 µM), EGTA (5 mM). Subsequent experiments were implemented in the presence of drug(s) within 15 min of incubation.

EF application and time-lapse recording
The direct-current EFs were applied as previously described (Zhao *et al.*, 1996; Song *et al.*, 2007) in custom-made electrotaxis chambers to minimize joule heating during the experiment. To eliminate toxic products from the electrodes that might be harmful to cells, agar salt bridges made with 1% agar gel in Steinberg's salt solution were used to connect silver/silver chloride electrodes in beakers of Steinberg's salt solution to pools of excess medium at either side of the chamber. The EF strength is based on the peak outward ionic currents in scale wounds that we measured using a vibrating probe, which averaged 3.52 µA/cm^2 (Figure 1E). The fish Ringer's solution that we used in the measurement has a conductivity (σ, which is the reciprocal of electrical resistivity) of about 13.74 m℧/cm (1.374 S/m), measured with a conductivity meter (VWR). A common approximation to the current density assumes that the current is simply proportional to the EF, as expressed by Ohm's law: $J_l = \sigma E$, where E is the EF. Plugging J_l and σ into the equation, we calculated that a density of 3.52 µA/cm^2 is equal to an EF of 2.56 V/cm. On the basis of our previous experience (Sun *et al.*, 2013), we used an EF of 2 V/cm in most experiments, unless otherwise stated. The actual voltage was measured by a voltmeter before and after each experiment. Phase contrast images were captured by a Zeiss Observer Z1 (Carl Zeiss) equipped with a QuantEM:512SC EMCCD camera (Photometrics) under a 10× lens. Time-lapse experiments were performed using MetaMorph NX software controlling a motorized scanning stage (Carl Zeiss). Typically, in each experiment, overlapped fields covering a whole cell group were captured sequentially. Images were taken at 30 or 60 s intervals at room temperature for up to 3 h, unless stated otherwise.

Image processing and data analysis
Time-lapse images were imported into ImageJ v1.53m and stitched by using the stitching plug-in. Tissue migration was tracked by monitoring centroid movement (see *Morphological extraction, quantification, and alignment* section below). Cell tracks were marked by using the MtrackJ tool and plotted by using the Chemotaxis and Migration tool v2.0, as described (Sun *et al.*, 2013).

Directionality (directedness) was defined as the cosine of theta, where θ is the angle between the displacement vector and the EF vector. The angle was quantified from the coordinates of each measured trajectory (Gruler and Nuccitelli, 1991; Tai *et al.*, 2009). If moved perfectly along the field vector toward the cathode, the cosine of this angle would be 1; if moved perpendicular to the field vector, the cosine of this angle would be 0; and if the cell moved directly toward the anode, the cosine of this angle would be −1. The migration speed was calculated using the trajectory arc length divided by the time. In some cases, electrotaxis experiments and subsequent quantifications were assigned in a double-blinded manner.

To visualize the migration, each object (cell or cell group) was numbered, and its *x* and *y* coordinates were measured on the first image and on every subsequent image in the image stack, with the *x*-axis parallel to the applied EF. The (*x*, *y*) data of each cell/group were imported by a custom MATLAB function and recalculated based on the optical parameters (lens and camera). Trajectories of the objects in each group were plotted in a Cartesian coordinate system by placing the first coordinates of each object to (0, 0).

Morphological extraction, quantification, and alignment

Phase contrast images (stitched or not stitched) were converted into binary images using custom-written MATLAB (The MathWorks) codes. Briefly, we used MATLAB edge detection and a basic morphology function to outline cells or groups in the phase contrast image. In most cases we had to use the Lasso tool in Photoshop (Adobe) to manually draw the cell or group shape. Polygonal outlines extracted from the binary images are plotted in Celltool, an open source software (Pincus and Theriot, 2007). Geometric features of each cell group including centroid, area, and aspect ratio were calculated directly from the polygons with a standard formula (Keren *et al.*, 2008). Serial polygonal outlines of a cell or cell group were extracted from time-lapse images and sampled at 200 evenly spaced points. These contours were then mutually and sequentially aligned to visualize collective cell motion over time (Pincus and Theriot, 2007). The number of cells within each keratocyte group was either counted using the ImageJ particle analysis tool or calculated based on the area fractions (Supplemental Figure S1, D and E).

PIV migration analysis

Collective keratocyte group migration in the time-lapse images was quantified by fast Fourier transform–based PIV analysis using PIVLab (Thielicke and Stamhuis, 2014) in MATLAB. Multiple iterations of interrogation window sizes were used (two iterations of 64×64 pixel windows followed by two iterations of 32×32 pixel windows). At each interrogation step, a 50% overlap was used. Vector validation excluded vectors beyond 5 SDs and replaced them with interpolated vectors. The resulting PIV vectors captured motions within the collective cell group and displacements on a timescale of 1 min. Spatial differences were inspected and visualized by color-coded surface plots. Kymographs were used to quantify and visualize spatiotemporal dynamics of velocity components parallel to the EF (u) and perpendicular to it (v) and directionality. For each data matrix from the PIV analysis, we computed the average value for each column parallel to the applied EF and then derived a one-dimensional segment for each time point using a custom MATLAB code, as previously described (Zhang *et al.*, 2017). To compare the drug effects, we also computed the time average of the u-velocity and directionality (cosθ) of each vector in each group during a certain period of EF application using the equation

$$\bar{u} = \frac{1}{T} \int_{(t_0)}^{(t_0+T)} u \, dt$$

where *u* is the u-velocity or directedness and *T* is the time counted from a fixed time point.

Immunostainings and fluorescence microscopy

Keratocyte sheets in custom-made EF chambers were fixed with 4% paraformaldehyde immediately or after EF application with field orientation mark, in the absence or presence of drugs by following procedures as described above. PIP3 was labeled with a mouse anti-PIP3 immunoglobulin G (Echelon; Z-P345b) followed by Alexa Fluor 532 goat anti-mouse 2nd antibody (Invitrogen) staining. F-actin was labeled by FITC-conjugated phalloidin (Sigma). Nuclei were labeled by Hoechst 33342. Images were taken in an inverted epifluorescence microscope. Images were stitched and processed using ImageJ. Quantification and comparison of fluorescence intensity were done in images taken in the same batch with the same optical setup and parameters. Nuclei in the cell clusters were detected using the "Surfaces" function in Bitplane Imaris software. "Touching" nuclei were separated using an object radius of 20 μm during thresholding based on total intensity. Matched average intensity for the PIP3 and Hoechst signals was extracted, and ratios were calculated, plotted, and analyzed using Microsoft Excel. Cells were counted using the particle analysis function.

Statistics and data availability

Data from representatives of at least four independent experiments are routinely presented as mean ± SE, unless stated otherwise. Student's *t* test and one-way analysis of variance followed by a post-hoc Tukey HSD test were used for paired or unpaired comparisons among two groups or multiple groups (more than two), respectively. ns: nonsignificant, $*p < 0.05$, $**p < 0.01$. MATLAB codes generated in this work are available upon reasonable request.

REFERENCES

Abercrombie M, Heaysman JEM (1953). Observations on the social behaviour of cells in tissue culture.1. Speed of movement of chick heart fibroblasts in relation to their mutual contacts. Exp Cell Res 5, 111–131.

Allen GM, Mogilner A, Theriot JA (2013). Electrophoresis of cellular membrane components creates the directional cue guiding keratocyte galvanotaxis. Curr Biol 23, 560–568.

Barker AT, Jaffe LF, Vanable JW (1982). The glabrous epidermis of cavies contains a powerful battery. Am J Physiol 242, R358–R366.

Barnes R, Shahin Y, Gohil R, Chetter I (2014). Electrical stimulation vs. standard care for chronic ulcer healing: a systematic review and meta-analysis of randomised controlled trials. Eur J Clin Invest 44, 429–440.

Barnhart E, Lee KC, Allen GM, Theriot JA, Mogilner A (2015). Balance between cell-substrate adhesion and myosin contraction determines the frequency of motility initiation in fish keratocytes. Proc Natl Acad Sci USA 112, 5045–5050.

Bonazzi D, Minc N (2014). Dissecting the molecular mechanisms of electro-tactic effects. Adv Wound Care (New Rochelle) 3, 139–148.

Caino MC, Ghosh JC, Chae YC, Vaira V, Rivadeneira DB, Faversani A, Rampini P, Kossenkov AV, Aird KM, Zhang R, *et al.* (2015). PI3K therapy reprograms mitochondrial trafficking to fuel tumor cell invasion. Proc Natl Acad Sci USA 112, 8638–8643.

Camley BA (2018). Collective gradient sensing and chemotaxis: modeling and recent developments. J Phys Condens Matter 30, 223001.

Castilho RM, Squarize CH, Gutkind JS (2013). Exploiting PI3K/mTOR signaling to accelerate epithelial wound healing. Oral Dis 19, 551–558.

Chang F, Minc N (2014). Electrochemical control of cell and tissue polarity. Annu Rev Cell Dev Biol 30, 317–336.

Chiang MC, Robinson KR, Vanable JW (1992). Electrical fields in the vicinity of epithelial wounds in the isolated bovine eye. Exp Eye Res 54, 999–1003.

Cho Y, Son M, Jeong H, Shin JH (2018). Electric field-induced migration and intercellular stress alignment in a collective epithelial monolayer. Mol Biol Cell 29, 2292–2302.

Cohen DJ, Nelson WJ, Maharbiz MM (2014). Galvanotactic control of collective cell migration in epithelial monolayers. Nat Mater 13, 409–417.

Cooper MS, Schliwa M (1985). Electrical and ionic controls of tissue cell locomotion in DC electric fields. J Neurosci Res 13, 223–244.

Cooper MS, Schliwa M (1986). Motility of cultured fish epidermal cells in the presence and absence of direct current electric fields. J Cell Biol 102, 1384–1399.

Cortese B, Palama IE, D'Amone S, Gigli G (2014). Influence of electrotaxis on cell behaviour. Integr Biol (Camb) 6, 817–830.

Dona E, Barry JD, Valentin G, Quirin C, Khmelinskii A, Kunze A, Durdu S, Newton LR, Fernandez-Minan A, Huber W, *et al.* (2013). Directional tissue migration through a self-generated chemokine gradient. Nature 503, 285–289.

Durant F, Bischof J, Fields C, Morokuma J, LaPalme J, Hoi A, Levin M (2019). The role of early bioelectric signals in the regeneration of planarian anterior/posterior polarity. Biophys J 116, 948–961.

Efimova N, Svitkina TM (2018). Branched actin networks push against each other at adherens junctions to maintain cell-cell adhesion. J Cell Biol 217, 1827–1845.

Etienne-Manneville S (2014). Neighborly relations during collective migration. Curr Opin Cell Biol 30, 51–59.

Farooqui R, Fenteany G (2005). Multiple rows of cells behind an epithelial wound edge extend cryptic lamellipodia to collectively drive cell-sheet movement. J Cell Sci 118, 51–63.

Friedl P, Gilmour D (2009). Collective cell migration in morphogenesis, regeneration and cancer. Nat Rev Mol Cell Biol 10, 445–457.

Gruler H, Nuccitelli R (1991). Neural crest cell galvanotaxis: new data and a novel approach to the analysis of both galvanotaxis and chemotaxis. Cell Motil Cytoskeleton 19, 121–133.

Henson JH, Yeterian M, Weeks RM, Medrano AE, Brown BL, Geist HL, Pais MD, Oldenbourg R, Shuster CB (2015). Arp2/3 complex inhibition radically alters lamellipodial actin architecture, suspended cell shape, and the cell spreading process. Mol Biol Cell 26, 887–900.

Hirata H, Gupta M, Vedula SR, Lim CT, Ladoux B, Sokabe M (2015). Actomyosin bundles serve as a tension sensor and a platform for ERK activation. EMBO Rep 16, 250–257.

Huang L, Cormie P, Messerli MA, Robinson KR (2009). The involvement of Ca2+ and integrins in directional responses of zebrafish keratocytes to electric fields. J Cell Physiol 219, 162–172.

Kennard A, Theriot J (2020). Osmolarity-independent electrical cues guide rapid response to injury in zebrafish epidermis. eLife 9, e62386.

Keren K, Pincus Z, Allen GM, Barnhart EL, Marriott G, Mogilner A, Theriot JA (2008). Mechanism of shape determination in motile cells. Nature 453, 475–480.

Khalil AA, Friedl P (2010). Determinants of leader cells in collective cell migration. Integr Biol (Camb) 2, 568–574.

Kloth L, Zhao M (2010). Endogenous and exogenous electrical fields for wound healing. In: Wound Healing: Evidence Based Management, ed. JM McCulloch and LC Kloth, Philadelphia, PA: F. A. Davis.

Kloth LC (2014). Electrical stimulation technologies for wound healing. Adv Wound Care (New Rochelle) 3, 81–90.

Kolsch V, Charest PG, Firtel RA (2008). The regulation of cell motility and chemotaxis by phospholipid signaling. J Cell Sci 121, 551–559.

Kovács M, Tóth J, Hetényi C, Málnási-Csizmadia A, Sellers JR (2004). Mechanism of blebbistatin inhibition of myosin II. J Biol Chem 279, 35557–35563.

Li J, Zhang S, Soto X, Woolner S, Amaya E (2013). ERK and phosphoinositide 3-kinase temporally coordinate different modes of actin-based motility during embryonic wound healing. J Cell Sci 126, 5005–5017.

Li L, Hartley R, Reiss B, Sun Y, Pu J, Wu D, Lin F, Hoang T, Yamada S, Jiang J, *et al.* (2012). E-cadherin plays an essential role in collective directional migration of large epithelial sheets. Cell Mol Life Sci 69, 2779–2789.

Lima MH, Caricilli AM, de Abreu LL, Araujo EP, Pelegrinelli FF, Thirone AC, Tsukumo DM, Pessoa AF, dos Santos MF, de Moraes MA, *et al.* (2012). Topical insulin accelerates wound healing in diabetes by enhancing the AKT and ERK pathways: a double-blind placebo-controlled clinical trial. PLoS One 7, e36974.

Lin F, Baldessari F, Crenguta Gyenge C, Sato T, Chambers RD, Santiago JG, Butcher EC (2008). Lymphocyte electrotaxis in vitro and in vivo. J Immunol 181, 2465–2471.

Mayor R, Carmona-Fontaine C (2010). Keeping in touch with contact inhibition of locomotion. Trends Cell Biol 20, 319–328.

McCaig CD, Rajnicek AM, Song B, Zhao M (2005). Controlling cell behavior electrically: current views and future potential. Physiol Rev 85, 943–978.

Meng X, Arocena M, Penninger J, Gage FH, Zhao M, Song B (2011). PI3K mediated electrotaxis of embryonic and adult neural progenitor cells in the presence of growth factors. Exp Neurol 227, 210–217.

Mogilner A, Barnhart EL, Keren K (2020). Experiment, theory, and the keratocyte: an ode to a simple model for cell motility. Semin Cell Dev Biol 100, 143–151.

Nakajima K, Zhu K, Sun YH, Hegyi B, Zeng Q, Murphy CJ, Small JV, Chen-Izu Y, Izumiya Y, Penninger JM, *et al.* (2015). KCNJ15/Kir4.2 couples with polyamines to sense weak extracellular electric fields in galvanotaxis. Nat Commun 6, 8532.

Nuccitelli R (2003). A role for endogenous electric fields in wound healing. Curr Top Dev Biol 58, 1–26.

Omelchenko T, Vasiliev JM, Gelfand IM, Feder HH, Bonder EM (2003). Rho-dependent formation of epithelial "leader" cells during wound healing. Proc Natl Acad Sci USA 100, 10788–10793.

Parent CA, Blacklock BJ, Froehlich WM, M DB, Devreotes PN (1998). G protein signaling events are activated at the leading edge of chemotactic cells. Cell 95, 81–91.

Pincus Z, Theriot JA (2007). Comparison of quantitative methods for cell-shape analysis. J Microsc 227, 140–156.

Poujade M, Grasland-Mongrain E, Hertzog A, Jouanneau J, Chavrier P, Ladoux B, Buguin A, Silberzan P (2007). Collective migration of an epithelial monolayer in response to a model wound. Proc Natl Acad Sci USA 104, 15988–15993.

Raja SK, Garcia MS, Isseroff RR (2007). Wound re-epithelialization: modulating keratinocyte migration in wound healing. Front Biosci 12, 2849–2868.

Rajnicek AM, Foubister LE, McCaig CD (2006). Temporally and spatially coordinated roles for Rho, Rac, Cdc42 and their effectors in growth cone guidance by a physiological electric field. J Cell Sci 119, 1723–1735.

Rapanan JL, Cooper KE, Leyva KJ, Hull EE (2014). Collective cell migration of primary zebrafish keratocytes. Exp Cell Res 326, 155–165.

Reid B, Nuccitelli R, Zhao M (2007). Non-invasive measurement of bioelectric currents with a vibrating probe. Nat Protoc 2, 661–669.

Richardson R, Metzger M, Knyphausen P, Ramezani T, Slanchev K, Kraus C, Schmelzer E, Hammerschmidt M (2016). Re-epithelialization of cutaneous wounds in adult zebrafish combines mechanisms of wound closure in embryonic and adult mammals. Development 143, 2077–2088.

Richardson R, Slanchev K, Kraus C, Knyphausen P, Eming S, Hammerschmidt M (2013). Adult zebrafish as a model system for cutaneous wound-healing research. J Invest Dermatol 133, 1655–1665.

Sato MJ, Kuwayama H, van Egmond WN, Takayama AL, Takagi H, van Haastert PJ, Yanagida T, Ueda M (2009). Switching direction in electric-signal-induced cell migration by cyclic guanosine monophosphate and phosphatidylinositol signaling. Proc Natl Acad Sci USA 106, 6667–6672.

Scarpa E, Mayor R (2016). Collective cell migration in development. J Cell Biol 212, 143–155.

Shellard A, Mayor R (2019). Supracellular migration—beyond collective cell migration. J Cell Sci 132, jcs226142.

Shellard A, Szabo A, Trepat X, Mayor R (2018). Supracellular contraction at the rear of neural crest cell groups drives collective chemotaxis. Science 362, 339–343.

Shi R, Borgens RB (1994). Embryonic neuroepithelial sodium-transport, the resulting physiological potential, and cranial development. Dev Biol 165, 105–116.

Shim G, Devenport D, Cohen DJ (2021). Overriding native cell coordination enhances external programming of collective cell migration. Proc Natl Acad Sci USA 118, e2101352118.

Song B, Gu Y, Pu J, Reid B, Zhao Z, Zhao M (2007). Application of direct current electric fields to cells and tissues in vitro and modulation of wound electric field in vivo. Nat Protoc 2, 1479–1489.

Sun Y, Do H, Gao J, Zhao R, Zhao M, Mogilner A (2013). Keratocyte fragments and cells utilize competing pathways to move in opposite directions in an electric field. Curr Biol 23, 569–574.

Sun YH, Sun Y, Zhu K, Reid B, Gao X, Draper BW, Zhao M, Mogilner A (2018). Electric fields accelerate cell polarization and bypass myosin action in motility initiation. J Cell Physiol 233, 2378–2385.

Szabo B, Szollosi GJ, Gonci B, Juranyi Z, Selmeczi D, Vicsek T (2006). Phase transition in the collective migration of tissue cells: experiment and model. Phys Rev E Stat Nonlin Soft Matter Phys 74, 061908.

Tai G, Reid B, Cao L, Zhao M (2009). Electrotaxis and wound healing: experimental methods to study electric fields as a directional signal for cell migration. Methods Mol Biol 571, 77–97.

Theveneau E, Marchant L, Kuriyama S, Gull M, Moepps B, Parsons M, Mayor R (2010). Collective chemotaxis requires contact-dependent cell polarity. Dev Cell 19, 39–53.

Thielicke W, Stamhuis EJ (2014). PIVlab—towards user-friendly, affordable and accurate digital particle image velocimetry in MATLAB. J Open Res Softw 2, e30.

Travis J (2011). Mysteries of the cell. Science 334, 1046.

Trepat X, Chen Z, Jacobson K (2012). Cell migration. Compr Physiol 2, 2369–2392.

Vedula SR, Hirata H, Nai MH, Brugues A, Toyama Y, Trepat X, Lim CT, Ladoux B (2014). Epithelial bridges maintain tissue integrity during collective cell migration. Nat Mater 13, 87–96.

Vlahos CJ, Matter WF, Hui KY, Brown RF (1994). A specific inhibitor of phosphatidylinositol 3-kinase, 2-(4-morpholinyl)-8-phenyl-4H-1-benzopyran-4-one (LY294002). J Biol Chem 269, 5241–5248.

Worley KE, Shieh D, Wan LQ (2015). Inhibition of cell-cell adhesion impairs directional epithelial migration on micropatterned surfaces. Integr Biol (Camb) 7, 580–590.

Yam PT, Wilson CA, Ji L, Hebert B, Barnhart EL, Dye NA, Wiseman PW, Danuser G, Theriot JA (2007). Actin-myosin network reorganization breaks symmetry at the cell rear to spontaneously initiate polarized cell motility. J Cell Biol 178, 1207–1221.

Yamaguchi N, Mizutani T, Kawabata K, Haga H (2015). Leader cells regulate collective cell migration via Rac activation in the downstream signaling of integrin beta1 and PI3K. Sci Rep 5, 7656.

Yoo SK, Deng Q, Cavnar PJ, Wu YI, Hahn KM, Huttenlocher A (2010). Differential regulation of protrusion and polarity by PI3K during neutrophil motility in live zebrafish. Dev Cell 18, 226–236.

Zajdel TJ, Shim G, Wang L, Rossello-Martinez A, Cohen DJ (2020). SCHEEPDOG: programming electric cues to dynamically herd large-scale cell migration. Cell Syst 10, 506–514.e503.

Zhang Y, Wu J, Lee RM, Zhu Z, Sun Y, Zhu K, Losert W, Liao S, Zhang G, Pan T, et al. (2022). Propagation dynamics of electrotactic motility in large epithelial cell sheets. iScience 25, 105136

Zhang Y, Xu G, Lee RM, Zhu Z, Wu J, Liao S, Zhang G, Sun Y, Mogilner A, Losert W, et al. (2017). Collective cell migration has distinct directionality and speed dynamics. Cell Mol Life Sci 74, 3841–3850.

Zhao M (2009). Electrical fields in wound healing—an overriding signal that directs cell migration. Semin Cell Dev Biol 20, 674–682.

Zhao M, Agius-Fernandez A, Forrester JV, McCaig CD (1996). Directed migration of corneal epithelial sheets in physiological electric fields. Invest Ophthalmol Vis Sci 37, 2548–2558.

Zhao M, Pu J, Forrester JV, McCaig CD (2002). Membrane lipids, EGF receptors, and intracellular signals colocalize and are polarized in epithelial cells moving directionally in a physiological electric field. FASEB J 16, 857–859.

Zhao M, Song B, Pu J, Forrester JV, McCaig CD (2003). Direct visualization of a stratified epithelium reveals that wounds heal by unified sliding of cell sheets. FASEB J 17, 397–406.

Zhao M, Song B, Pu J, Wada T, Reid B, Tai G, Wang F, Guo A, Walczysko P, Gu Y, et al. (2006). Electrical signals control wound healing through phosphatidylinositol-3-OH kinase-gamma and PTEN. Nature 442, 457–460.